

Evidence of Structural Distortions in Mixed Mn-Znferrite

A. F. L. Moreira*, F. L. O. Paula, J. Depeyrot

Institute of Physics, University of Brasilia, 70919-970, Brasilia, Brazil

Corresponding Author: A. F. L. Moreira

Abstract: We investigate the local structure of nanoparticles based on a manganese-zinc ferrite. Results of X-ray powder diffraction (XRD) analyzed by Rietveld Refinement and X-ray Pair Diffraction Function (PDF) measurements are crossed with those of magnetization curves and Near Structure X-ray absorption spectroscopy (XANES) to study the valence state of Mn ions and the cation distribution at interstitial sites of nanoparticle structure. Linear combination fitting of XANES data clearly indicates the existence of mixed valence states of Mn cations. Thus, it induces nonequilibrium cation distributions in the nanoparticle with the presence of a large amount of Mn cations at octahedral sites. The results of Rietveld, PDF and magnetism are in good agreement and also show an octahedral distortion.

Keywords: Pair Distribution Function; Rietveld; Mixed Ferrite Mn-Zn.

Date of Submission: 30-04-2019

Date of acceptance: 15-05-2019

I. Introduction

In nanotechnology research, a material that has been very important are so-called ferrofluids, which are colloidal dispersions of magnetic nanoparticles, with sizes of the order of few nanometers, in a liquid carrier. These ferrofluids, after adequate surface functionalization, can be dispersed in several biological media, aiming at the cellular separation, obtaining of magnetic resonance images, to the cancer treatment (inside the tumors) by magnetic hyperthermia [1,2]. In addition, spinel-type ferrite nanoparticles, in particular Mn-Zn nanoparticles, represent a group of the most widely used flexible magnets in many technological applications such as electronics [3]. For example, throttling coils, loudspeaker, recording heads, broadband pulse transformers, etc.

Spinel ferrites with general molecular formula MFe_2O_4 , M being a divalent transition metal, crystallize in a face-centered cubic lattice ($Fd\bar{3}m$) that corresponds to a close-packed arrangement of 32 oxygen anions, with 64 tetrahedral interstices (A sites) and 32 octahedral interstices (B sites). The metallic cations only occupy 1/8 of the A-sites and 1/2 of the B-sites and the crystallographic representation $[M_{(1-x)}^{2+}Fe_x^{3+}]_A[M_x^{2+}Fe_{(2-x)}^{3+}]_B O_4^{2-}$ is better chosen to clearly express the cation distribution among the tetrahedral and octahedral sites. In this case x is called inversion degree and is the fraction of A-sites occupied by Fe^{3+} cations or the fraction on B sites occupied by divalent metals. If x is zero the structure is named normal spinel as for $ZnFe_2O_4$ bulk material and when x equals one it is an inverse spinel like ideal $CoFe_2O_4$ structure. However, in ferrite nanoparticles the spatial confinement at the nanometric scale leads to underlying cubic lattices that often present non-equilibrium cation distributions [19,20]. In such a context it is necessary to perform experiments able to enlighten the very local structure of these nanocrystals.

Ferrofluids constituted by Mn-Zn nanoparticles may be good candidates for liquids carrying heat exchange devices using magnetocaloric energy conversion [4]. In this purpose, we investigate the properties that give rise to this great variety of possible applications, properties like crystalline structure, the use of specific ions in the structure can be very important in the magnetism of these nanosystems. The present work deals with the synthesis of nanoparticles (NPs) type Ferrite Mn-Zn by co-precipitation method and structure of crystalline characterization using three synchrotron techniques, Powder X-Ray Diffraction (XPD), X-Ray Extraction Edge (XANES), Pair Diffraction Function (PDF) and Vibration Sample Magnetometer (VSM).

II. Experimental

2.1 Sample Preparation

The spinel $Mn_{0.9}Zn_{0.1}Fe_2O_4$ (sample MZ1) nanoparticles (NPs) are synthesized by hydrothermal co-precipitation [5], of initial aqueous solutions mixtures (0.5M) of $MnCl_2 \cdot 4H_2O$, $ZnCl_2$ and $FeCl_3 \cdot 6H_2O$, in a solution proportion 1(divalent metals):2(iron trivalent). Synthesis does not occur at room temperature and reagents have to be brought to a boil. In this way, an alkaline solution (NaOH - 0.7M) was heated at 100°C and the divalent metal solution was heated to 60°C. After reaching these temperatures the addition of the divalent metal solution to the base solution was done. After the mixture reached the boiling temperature again, the reaction was continued for another 30 minutes under stirring and boiling. In order to prevent $FeCl_3$ hydrolysis at this temperature, acid is added to initial mixtures, showed that the results on the yield of the synthesis are not

altered by the type of acid used (H_2SO_4 , HNO_3 , HCl or HClO_4) in order to prevent hydrolysis in the initial mixture, however acid concentration acts also on size and polydispersity. Reagent addition procedure acts on the particle size, especially the way and the rapidly of reagent mixing. The synthesis report in order to get the great grains are obtained by pouring the Mn(II)Zn(II)-Fe(III) mixture as slowly as possible into base solution under slow stirring. The nature of the base acts significantly on the size of the ferrites. Thus, the type and the molar concentration [5] were chosen favoring a higher crystalline growth of the nanoparticles. To perform the addition of the reagents, a burette with a flow rate of 3 mL/s was used ensuring a slow addition. In addition, to minimize the oxidation of Mn^{+2} the solutions were exposed to the N_2 gas flow before and throughout the reaction. As a summary, co-precipitation step performed at 100°C is then largely influenced by several parameters. Therefore, particle size and polydispersity depend on the operating mode, on the nature of precipitating base and on the initial mixture acidity. Control of these parameters allows reproducible results to be obtained nanoparticles with relatively larger sizes. After the reaction time, the precipitate is washed in water and treated with HNO_3 solution 2M to reduce the co- and opposite ion concentrations and to clean the particle surfaces. After, the precipitate is washed in water and drying. The nanoparticles powders analyzed in this work are obtained after evaporation of the aqueous liquid.

2.2 Measurements

At last step of the synthesis, the [Fe], [Mn] and [Zn] content in the nanoparticles is investigated at University of Brasilia – Brazil with a Shimadzu EDX 720HS - Spectroscopy Dispersive X-ray (EDX). The physical chemical properties of the nanoparticles have been determined by combining Synchrotron X-Ray Diffraction (XRD), Pair Diffraction Function (PDF) and X-ray Absorption Near Edge Structure (XANES) measurements. In addition, the magnetic properties were studied with measurements in a Vibrating Sample Magnetometer (VSM). The sample has a Wyckoff Positions of $Fd\bar{3}m(\text{No.}227:2)$. Then, in this work, we have obtained a precipitate containing NPs with mean size around 24 nm. For XRD, PDF and XANES, the data processing, optics and the main characteristics of the XDS beamline (W09A-XDS) of the LNLS set up could be found in a refer [6]. The PDF data were collected in transmission mode at room temperature, with a point scintillator detector (FMB-Oxford LaBr). The focusing element was a toroidal mirror and the incident beam was a “bow tie” format. In this configuration, unwanted background arising from external sources and Compton scattering is minimized. The employed wavelength was 0.6199 \AA ($\sim 20 \text{ keV}$). The samples were measured in the 3 ranges between 1 and 60; 60 and 120; 120 and 160 with different steps 0.004, 0.006 and 0.008 in 2θ , respectively, with $Q_{\text{max}} = 20.0 \text{ \AA}^{-1}$. The diffracted lines are related to the characteristic interplanar spacings of the structure and compared with bulk standard data of the International Centre for Diffraction Data (ICDD) for MnFe_2O_4 (ICDD no. 01-073-1964), ZnFe_2O_4 (ICDD no. 98-007-2033), $\text{Zn}_{(1-x)}\text{Mn}_x\text{Fe}_2\text{O}_4$ (ICDD no. 98-002-8512 to -8516). The data were normalized for incoming beam intensity, employing a monitor detector to count a fixed number of photons for each angle. The XRD data was collected in the same conditions. We measured the sample MZ1 and the alumina standard (Al_2O_3 ; NIST 676) inside 0.15 mm polyimide capillary tubes (KAPTON[®]) at the XDS beamline [7]. The samples were mounted inside the capillary tube on a stainless-steel base fixed with beeswax. They rotate on their own axis, in the direction perpendicular to the beam and the scintillator. The background was determined by measuring an empty capillary under identical experimental conditions. XANES spectra are collected in transmission mode, at room temperature, around the Mn K-edge. Each spectrum corresponds to an average over three independent scans. Magnetization measurements are performed at UnB at using the model of Vibrating Sample Magnetometer (VSM - PPMS- Physical Property Measurement System, Quantum Design mod. 6000). Magnetization curve as a function of temperature in the presence of a field of 50 kOe.

2.2.1 PDF Data processing and analysis

The X-ray diffraction measurements was performed at room temperature over the range in r space between 1.4 and 30 \AA . The intensity data were corrected and normalized using the program PDFgetX2 [8] to obtain the total scattering structure function, $F(Q)$, and its sine Fourier transform, i.e. the atomic PDF, $G(r)$. This Python-based software uses a data correction method, where the slowly changing structure-independent signal is filtered out to obtain X-ray intensities that contain structure information. Corrections performed by PDFgetX2 include, for example, for incoherent Compton scattering, background scattering from the sample container/air, sample self-absorption, polarization of the X-ray beam, etc. In the Fourier transform of $F(Q)$ to obtain $G(r)$, the data were truncated at a finite maximum value of the ($Q = Q_{\text{max}}$) momentum transfer. Q_{max} was optimized so as to avoid large termination effects and to reasonably minimize the introduced noise level as the signal to noise ratio decreased with the increased Q value. Here, $Q_{\text{max}} = 20.0 \text{ \AA}^{-1}$ was found to be optimal. To verify possible local structural characteristics, especially due to the peculiar cubic shape, PDF analysis was applied. First, PDF data from the alumina standard (Al_2O_3 ; NIST 676) sample were modeled up to 500 \AA to obtain Q_{damp} and Q_{broad} , which describe experimental resolution effects. The PDF data modeling resulted in $Q_{\text{damp}} = 0.058 \text{ \AA}^{-1}$ and $Q_{\text{broad}} =$

0.005 \AA^{-1} , which were kept fixed during the subsequent fitting procedures. For the PDF [9] data modeling of the sample, cell parameters, isotropic atomic displacement parameters, atomic positions, and the parameter Δ_2 (which accounts for correlated atomic motion effects in PDFgui[10]) were refined. We fitted all the structural parameters, maintaining the symmetry of the compound. We also adjusted the scale factor, the Gaussian damping factor (Q_{damp}) and the peak broadening.

2.2.2 XRD Data processing and analysis

Preliminary analyses were performed using the Williamson-Hall method, to determine the strain size. In order to make the analyses, Rietveld structure refinement of the XRD data is performed using the GSAS software package developed by Larson and Von Dreele[11]. It provides a fitting procedure of experimental results and allows determining here the lattice parameter, the oxygen position, and the cation distribution (x) that represent the Fe^{3+} occupation at the tetrahedral site. The structure refinements are made with a peak shape modeled by a pseudo-Voigt function that includes correction for peak asymmetry and background intensity well accounted by a Chebyshev polynomial function. The diffractogram was fitted until the convergence for the data, the best result being selected on the basis of reliability factor of refinement (R_{wp}) and Goodness of Fit (GOF). The results of the refinements carried out on this powder are listed in table 2. For the refinement we begin first with the background factors in which we used Chebyshev function with only 3 terms. In the next step the following parameters were refined: cationic distribution, oxygenic occupation, lattice parameters, size, and strain.

2.2.3 XANES Data processing and analysis

XANES spectra are collected in transmission mode, at room temperature, at the LNLS W09A-XDS beamline [6] around the Mn K-edge. The spectrum corresponds to an average over three independent scans. The spectra are calibrated in energy by measurements of transmission spectra of Mn foils. The energies E_0 was defined like the maximum of the first derivation at the absorption edge of these reference sample is 6552 eV [12]. Background removal is performed by means of the AUTOBK algorithm. In the absence of the bulk material, the oxides (Mn_2O_3 , MnO_2 , Mn_3O_4) were used to adjust the experimental data. Thus, in this form the data directly reflect the average local environment around the absorbing atoms.

2.2.4 Magnetic Data processing and analysis

Magnetization measurements are performed at UnB (Physics Institute) using the vibrating sample magnetometer (VSM; PPMS, Quantum Design model 6000). Magnetization curves are obtained as a function of the applied field (up to 9000 kA/m), between 5 K after a zero-field-cooling (ZFC) procedure and at 300 K. The signals of magnetization were normalized by the sample mass and multiple by the density of the nanoparticle. The water signal was subtracted. Thus, with the obtained signals for the magnetic hysteresis and the coercivity field versus temperature was analyzed to take the value of saturation magnetization and the Block temperature, respectively.

III. Results

Energy Dispersive X-ray (EDX) spectroscopy was used to determine a chemical composition of the sample. The Fig. 1 show the results of EDX plotted at a relative frequency scale. The value obtained for a fraction of divalent metals, $\chi^{\text{EDX}} = 0.34$, that is a percentage of Zinc and Manganese metals divided by a total quantity of metals, is close to the standard value for an ideal ferrite, that is 0.33. Table 1 shows the percentage values of the metal type obtained from EDX. The second plot of the Fig. 1 present broadening of the Full Width at Half Maximum (FWHM), β , of the X-ray diffracted peaks with the increasing of 2θ scattering angle. We can see the difference between the Bragg peaks (111), (311), (400) and (440). Thus, this is associated to the strain and the quantitative analyses was obtained using the Williamson-Hall method (W-H) [13]. Strain-induced broadening arising from crystal imperfections and distortion are related by $\varepsilon \approx \beta/\tan\theta$. This method allows a separation of reflection broadening and the strain. The third plot of the Fig. 1 shows the W-H analyses for the MZ1 sample and the Alumina standard sample. The slope of the plotted lines means the strain of the samples. The Alumina sample present a very lower value of the strain, 3.10^{-4} [14] and was used to subtract an instrumental error ($\beta_{\text{instrumental}}$). The W-H equation is:

$$\beta \cos\theta = \frac{\lambda}{D_{\text{RX}}^{\text{W-H}}} + 4S \sin\theta \quad (1)$$

where S is the Strain, $D_{\text{RX}}^{\text{W-H}}$ is the diameter and $\beta = \beta_{\text{measured}} - \beta_{\text{instrumental}}$. The Table 1 summarize the results to W-H analyses and the value of the strain (ε) is a typical to ferrite nanoparticles [19].

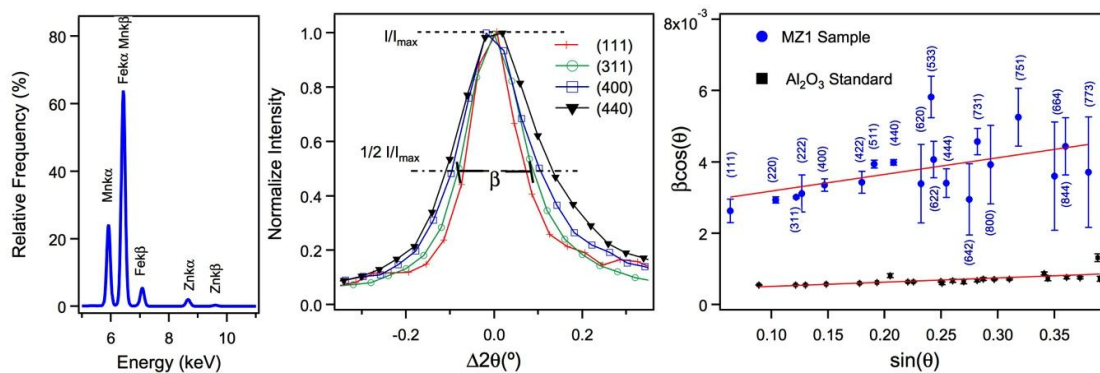


Figure 1. Elemental analysis of sample MZ1: performed by EDX; plot normalize intensity of X-ray diffraction by relative position; and the Williamson-Hall methodplot.

Table 1

$\chi^{EDX} = [M]/([M]+[Fe])$ being $M = Mn$ and Zn ; in the analysis of Williamson-Hall D_{RX}^{W-H} is the diameter and ε is Strain;

% Mn	% Zn	% Fe	χ^{EDX}	D^{W-H} (nm)	ε
29.78	3.82	65.30	0.34	23.19	1.19×10^{-3}

Fig. 2 show the X-ray diffraction pattern after the Rietveld refinement of MZ1 data. The Miller's indices were shown for thirty-one peaks. The blue circle symbols are the experimental data, the red solid line represent the fit and the green solid line are the difference between the experimental and fit line. The last show a good quality of fit and could be represented by the values of GOF (χ^2) and Rwp . Table 2 summarize the results of the Rietveld Refinement analyses for our sample. The values obtained for the cell parameter, oxygen position and for the quality of fit: GOF and reliability factor are showing and are below the acceptable limits seen in the literature [15]. The Rietveld refinement results show that the nanoparticle structure is spinel as was predict.

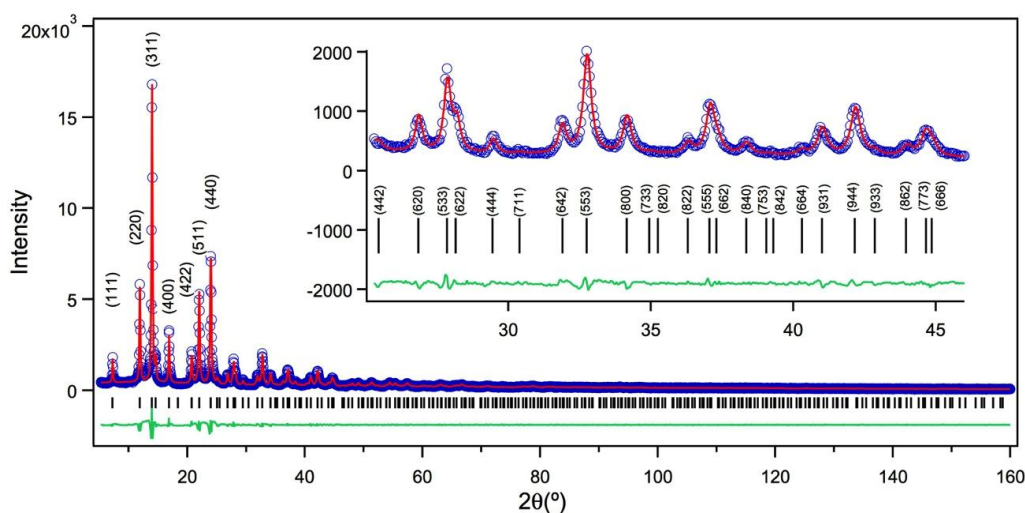


Figure 2: X ray diffractogram of the MZ1 sample showing the experimental points (o), the adjust done by the GSAS program (solid line) and right above the difference between the experimental points and the adjust done by the refinement.

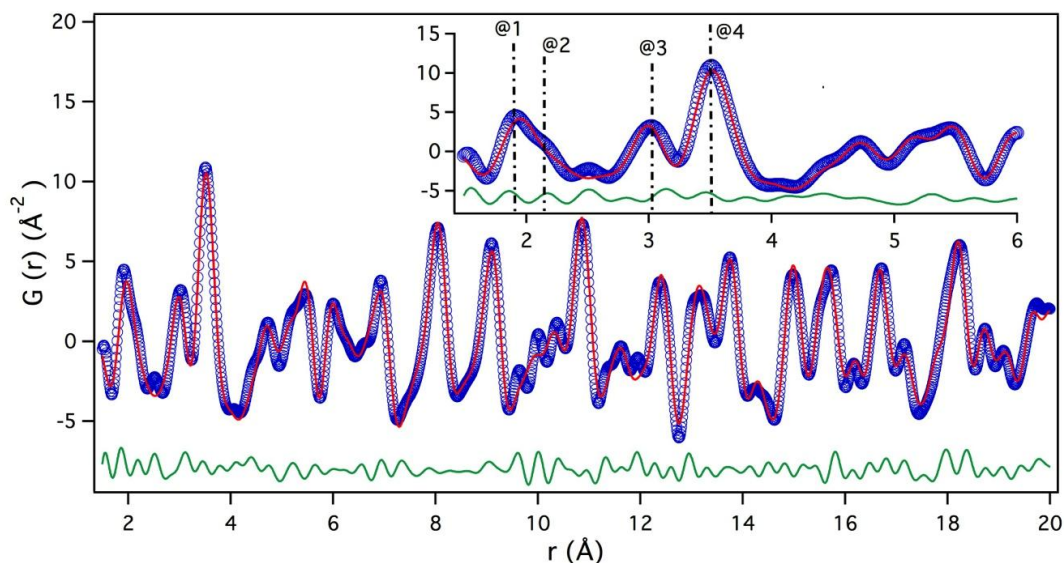


Figure 3. Pair Diffraction Function (PDF) Refinement of the MZ1 sample data with the $Fd\bar{3}m$ (SG. 227: 2) group space (red solid line) at 300 K. The blue symbols are the experimental data. The green solid line represents the difference between the experimental and the refinement. The insert shows three first layers of coordination. The peak position is marked by a vertical dotted line.

The Fig. 3 shows the radial distribution function, $G(r)$, obtained from the diffraction data by Fourier transforming the normalized total structure factor $S(Q)$ with $Q=4\pi(\sin\theta)/\lambda$. $S(Q)$ is the measured intensity corrected for background, Compton and multiple scattering, absorption, geometric and other factors. The inset in Figure 3 shows the enlargement of the region until 6 Å where 4 points are highlighted. In order the position @1 around 1.90 Å is physically understood like the distance between the oxygen atoms and the centered metal ions of the A site ($M(A)-O$). The position @2 around 2.10 Å represent the distance between the oxygen atoms and the centered metal ions of the B site ($M(B)-O$), @3 ($M(B)-M(B)$) and @4 ($M(A)-M(B)$) one arises from the scattering by the second coordination shell and the distances around 3.0 Å and 3.5 Å represent the near-neighbor metal-metal ions in the octahedral site and A-B sites, respectively, and the Table 2 summarizes these values. The values of the structural parameters obtained for PDF analysis, lattice parameters (a) and oxygen coordinates (u), are in reasonably good agreement with those determined from the Rietveld, see Table 2.

Table 2

Rietveld and PDF refined results

	a (Å)	u	$M(A)-O$ (Å)	$M(B)-O$ (Å)	$M(B)-M(B)$ (Å)	$M(A)-M(B)$ (Å)	x	χ^2	R_{wp}
Rietveld	8.43(8)	0.255(2)	1.90(6)	2.06(5)	2.98(3)	3.48(1)	0.78(1)	2.81	0.094
PDF	8.43(4)	0.255(1)	1.91(1)	2.10(1)	2.99(0)	3.50(1)	0.79(1)	2.08	0.179

Fig. 4 shows the Mn K-edge XANES spectra collected at room temperature and in the same conditions for the oxides. The energy edge deduced from the spectra shows, as expected, that the average valence of Mn ions in the synthesized nanoparticles samples is varied between +2 and +4 but the mean value is +3.

To determine the valence state of the MZ1 nanoparticles was analyzed the XANES of the oxides Mn_3O_4 , Mn_2O_3 , MnO_2 by applying the Linear Combination Fitting (LCF) method to the spectra of MZ1 nanoparticles sample. In such calculations, the XANES spectrum of the nanoparticles is analyzed considering a linear combination of XANES spectra obtained from oxides samples. The quality of the fit corresponds to low R factors ($< 1\%$) and the result points out to the proportions, 26% of MnO_2 and 18% of Mn_2O_3 and 57% of Mn_3O_4 . The oxidation of Mn in these oxides is known like +4, +3 and a mix of +2 and +3 respectively. The oxidation of the oxide Mn_3O_4 has the proportion known like 33% of +2 and 67% [16] of +3 leading to a 56% of Mn^{3+} . Such result means that there is more Mn^{3+} than other valence states in the MZ1 sample resulting in an average Mn oxidation equal +3.1.

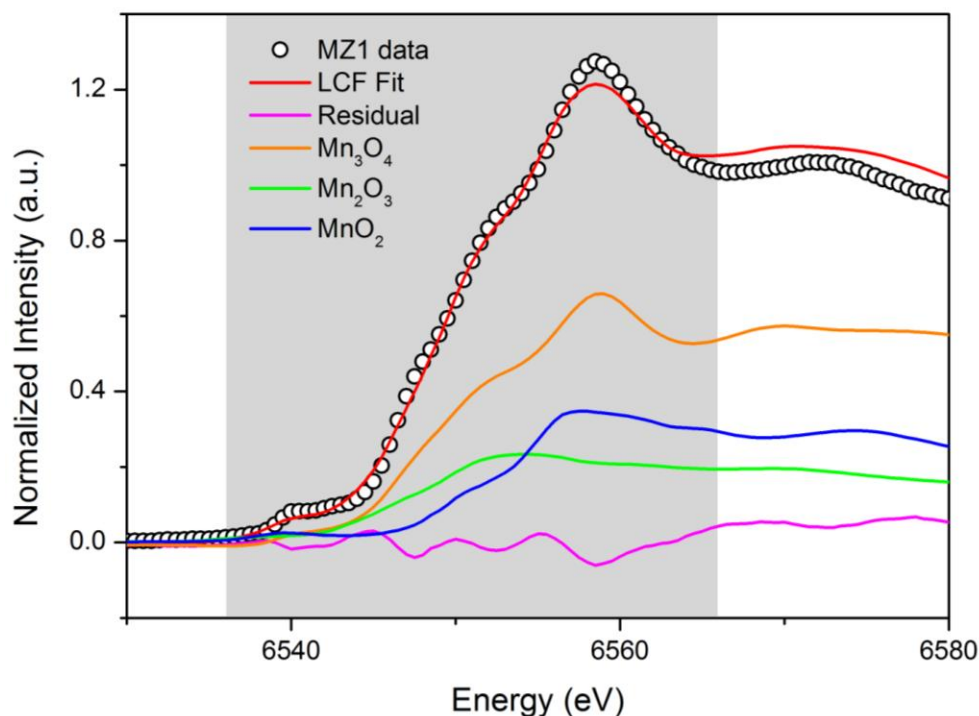


Figure 4. Experimental XANES spectra of the MZ1 sample (open circles) fitted (red full line) using a LCF of experimental XANES spectra of MnO₂, Mn₂O₃ and Mn₃O₄ oxides. Residual is also shown as the lowest trace (pink full line).

Table 3

Analyze using Bloch's law (\dagger); and by analysis using Kneller's law (\S).

$\dagger M_0$ (kA/m)	$\dagger B$	$\dagger \alpha$	$\S T_B$ (K)	$\S M_s$ (kA/m)	$\S K$ (J/m ³)
411	7.76×10^{-5}	1.5	302.93	411.5	1.8×10^4

The Fig.5 shows a typical magnetization result obtained for MZ1sample. The value of saturation magnetization M_s was measured at 5K and 300K at maximum field (9000kA/m). To determine the value of experimental saturation magnetization (see Table 3) we set using Bloch's law $T^{3/2}$ [17] and find M_s value around 411 kA/m and a value of coefficient α typical of 1.5 for bulk systems. This coefficient is size dependent and independent of the structure. To adjust the fitted curve, we set free this coefficient and find the same value. Set the temperature scale like log natural the linear behavior was observed for MZ1 sample of Bloch's Law ($M_s = M_0[1 - BT^\alpha]$), where M_0 is the magnetization at 0K, B is the Bloch constant, α is an adjustable parameter. This show a good agreement with the Bloch theory analyses. Using Kneller's Law [18],

$$H_c = 0.48 \frac{2K}{\mu_0 M_s} \left[1 - \left(\frac{T}{T_B} \right)^{\frac{1}{2}} \right] \quad (2)$$

where $\mu_0 = 4\pi \times 10^{-7} \text{ Tm/A}$, (T_B) is the block temperature, K is the anisotropy constant, we analyze the behavior of the curve coercivity field H_c vs temperature T and determine the Block temperature of this system with the value equal 302 K. The middle figure of Fig. 4 shows the decreasing behavior of remanence magnetization M_r as a function of temperature, with a higher decay up to the temperature 50K. Table 3 summarize the results of the analyze using Bloch's law and Kneller's law.

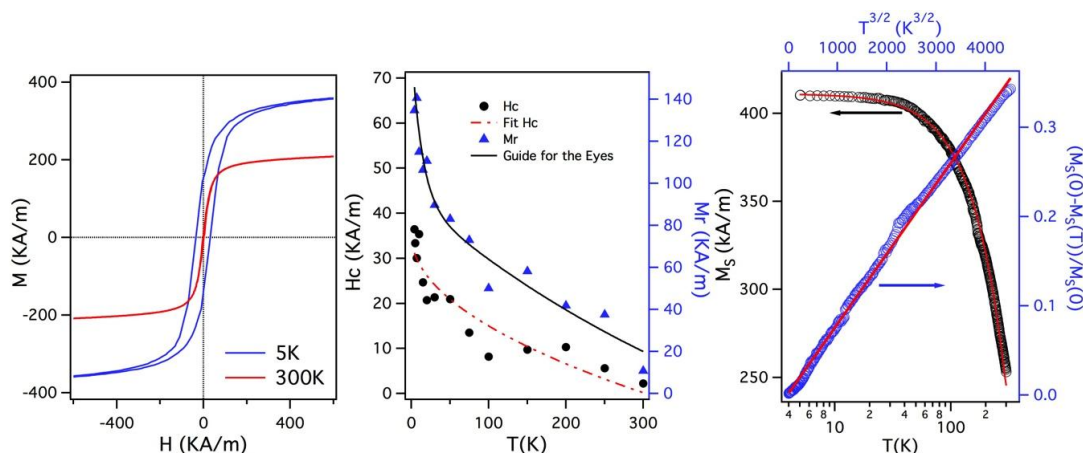


Figure 5. Hysteresis loops of MZ1 at 5K and 300K; Adjust using Kneller's law (H_c vs T) and Bloch's Law.

IV. Discussion

In the MZ1 sample using Williamson-Hall analyzes, we see an increase in the $\beta\cos\theta$ error of the peak (440) explained by the difficulty in determining the position and the width of the peak, since many of these peaks overlap. The same observation could be observing at the Bragg peak (222), which is very close to that of (311). Thus, we need to choose the peaks carefully to avoid overlapping peaks. This problem occurs in nanomaterials because the peaks are very large when compared to the bulk material. For example, the alumina sample shows no increase in error. The tensile effect is evident in the middle of Fig. 1 with increasing peaks which show a distortion of the network parameter in the nanoparticles. The XRD pattern shows good sample crystallinity as evidenced by the Rietveld Refinement up to the index peak (666) and a cubic packaging $Fd\bar{3}m$. Table 2 presents the fraction of Fe^{3+} ions at sites A with $x \sim 0.78$ and should be analyzed from the crystallographic formula of spinel-type ferrite. The cationic distribution determined by the techniques of this work shows good accuracy in the distribution between the sites, with $\sim 7\%$ of the zinc ions, $\sim 15\%$ of the manganese ions and $\sim 78\%$ of the iron ions being in the tetrahedral site. Thus, the cationic distribution for the refinement of the PDF is $[Mn_{0.14}Zn_{0.07}Fe_{0.79}]^A[Mn_{0.76}Zn_{0.04}Fe_{1.22}]^B O_{4.47}$ and for the refinement of Rietveld $[Mn_{0.15}Zn_{0.07}Fe_{0.78}]^A[Mn_{0.75}Zn_{0.04}Fe_{1.23}]^B O_{4.47}$. In previous studies [19, 20] we have seen that in zinc ferrites we had 64% occupancy at site A and in manganese ferrites we had 33% of Mn at site A. In the case of manganese ions, their occupation may be strongly associated with the valence state of the ions and the finite particle size [20]. The choice on δ , the oxidation parameter, was for to describe only one non-stoichiometric $MnZnFe_2O_{4+\delta}$ structural phase to take into account chemical titrations and electroneutrality[21]. The extra electronegative charge that appears per unit of formula exactly compensates for the positive charges coming from the oxidation of Mn ions, leading to $\delta = 0.47$. This approach also corresponds to the following chemical formula, $Mn_{0.8}Zn_{0.10}Fe_{1.8}O_4$, and produces vacancies with Fe and divalent cations in the proportion of 1: 2, distributed randomly at both interstitial sites by the adaptation procedure.

We see a good agreement with the diameter determined with the Williamson Hall method (23.19 nm) and with these refined by Rietveld (24.4 nm) and PDF (25.0 nm). The values of the position of the oxygen ion in both spinel phases are not exactly those corresponding to a perfect compact cubic packaging since they differ from the expected value 0.25 in the spatial group (No. 227: 2). The value found by the theoretical calculation performed in the rigid sphere model does not take into account the filling of the interstitial sites by metallic cations that can induce a slight distortion in the positions of the oxygen ions. In this work the position of the oxygen values, $u = 0.255$, refined by Rietveld and PDF method are in good agreement with the expected like have seen in the literature [19] for ferrite nanoparticles. For the refinements made, the amplitude average square of the atomic vibration in the equilibrium position (U_{iso}) was determined in both techniques and present a good agreement for the value found, $0.009 / 0.007 \text{ \AA}^2$ for metal ions at sites A, $0.010 / 0.012 \text{ \AA}^2$ for metal ions at sites B and $0.039 / 0.029 \text{ \AA}^2$ for oxygen ions respectively for Rietveld / PDF.

The results of the PDF show that there is a marked difference between the adjusted and experimental position @2, 2.10 Å and 2.20 Å, respectively. This discrepancy did not see for the other distances. Thus, this could indicate that a distortion in the octahedral sites made the distance in that direction longer than expected and the refinement cannot adjust this type of deformation that occurs in a direction of the octahedron site. In the LCF of the XANES spectra we observed that the oxidation state of the manganese ion is $\sim +3$. The XANES spectrum has a shoulder around 6552 eV, which is a characteristic related to a distortion of the MnO_6 octahedron. Other studies [22, 23], on manganese-based ferrite nanoparticles obtained by coprecipitation synthesis, present this shoulder related to the Jahn-Teller effect. Our sample has a majority proportion of Mn^{3+} (55%) and the XRD Rietveld Refinement and PDF analyzes show that B sites are predominantly occupied by

Mn ions. These shoulder-associated results seen in the XANES LCF around 6552 eV are good evidence that there is a Jahn-Teller effect in our sample. In the spinel-type ferrites, the metal cations located at sites A and B occupy the nodes of two spins subnets and the interaction of superexchange between them favors the antiparallel alignment of the spins. However, as described earlier there is a difference between the number of sites A and B and the way they are occupied, so this general behavior is described as ferrimagnetic. Then, if the distribution of metal cations within the A and B sites and the magnetic moment of each ion are known, the ferrite saturation magnetization at $T = 0$ K writes:

$$M_S = (Nd/M_M) \left[\sum_B n_{B,B} - \sum_A n_{B,A} \right] \mu_B \quad (3)$$

where $n_{B,i}$ is the number of Böhr magnetons, μ_B , associated with the i site of the unit cell, M_M is the molar mass of ferrite, d its density, and N is Avogadro's number. The summation extends over the A and B sites of the unit cell. In nanocrystals based on spinel ferrites, cation redistribution can modify significantly the properties of saturation magnetization when compared to bulk material. Thus, it would be theoretically possible to deduce the M_S if we have the inversion degree x from the value of PDF and the average number of oxidation of the Mn ions from XANES LCF. We therefore performed magnetization measurements at low temperature (5 K) in order to compare the M_S experimental and deduced from the equation (3). The deduced $M_S = 571.7$ kA/m value was found using $x = 0.78$ from Table 2, average oxidation number of Mn equal to 3.1 and volume fraction of the investigated nanoparticle. When compare these large and unexpected M_S deduced and experimental M_S value, the great difference could be associated with the reasons that the equation (3) does not take into account like the fact that the spin disorder on the surface of the nanoparticles [24]. This lack of alignment of the surface turns even in high fields, leading to a decrease in total magnetization. Another fact is the spin canting [25] that happens when the magnetic contribution of site A is very small in comparison to site B. This generates an increase of the B-B sites interaction in detriment of the decrease of the magnetic A-B sites interaction, causing a change in the magnetic structure [26]. In addition, the large difference between the values of M_S deduced and experimental may be related to a structural distortion, the Jahn Teller effect. This distortion caused at the B site can generate a drastic decrease in saturation magnetization. This distortion may be the main reason for the large difference in M_S .

V. Conclusion

The synthesis by the hydrothermal co-precipitation method presents a favorable technique to obtain the Mn-Zn ferrite with high crystallinity and nanostructured. A production was achieved in 100% of a cubic spinel phase and a single crystalline phase as evidenced by XRD Rietveld Refinement. The inversion degree was found ~ 0.8 for the XRD Rietveld Refinement and PDF showing a good agreement between the techniques. The mean diameter was found around 24 nm by Williamson-Hall analyses, Rietveld Refinement and PDF analyses. The atomic distance between the cation-oxygen in the B-site is longer for observed data than the adjust by PDF analyses pointing out a distortion of B-site. This difference was not found at other distances. In the LCF of the XANES spectra we observed that the oxidation state of the manganese ion is $\sim +3$. Near 6552 eV there is an evident shoulder in the XANES spectrum associated with the distortion of the octahedron MnO_6 . The theoretical saturation magnetization is greater than experimental suggesting that there is a distortion in the magnetic structure. Therefore, there are many evidences about Jahn Teller effect in our sample. In the future, this effect and the cationic distribution of Mn atoms and their oxidation states can be more enlightened by Diffraction Anomalous Fine Structure (DAFS) and X-ray Photoelectron Spectroscopy (XPS) studies.

Acknowledgements

This work was supported by Brazilian agencies, the National Council for Scientific and Technological Development through the National Institute of Science and Technology of Complex Fluids (INCT-FCx-CNPq – 465259/2014-6), the Coordination for the Improvement of Higher Education Personnel (CAPES) and the Federal District Research Foundation (FAPDF – 0193-001376/2016 and 0193-001194/2016). We also thank the Brazilian Synchrotron Light Laboratory (LNLS) for time measurements at beamline (W09A-XDS – proposal 16164). We are also grateful for the use of multiuser equipment of Vibrating Sample Magnetometer (VSM - PPMS- Physical Property Measurement System, Quantum Design) at the Institute of Physics at the University of Brasilia.

References

- [1]. V Pilati, R Cabreira Gomes, GS Gomide, P Coppola, FG Silva, FLO Paula, R Perzynski, GF Goya, R Aquino, J Depeyrot, "Core/shell Nanoparticles of Non-Stoichiometric Zn-Mn and Zn-Co Ferrites as Thermosensitive Heat Sources for Magnetic Fluid Hyperthermia", *Journal of Physical Chemistry C*, 122, 2018, 3028.
- [2]. QA Pankhurst, NTK Thanh, SK Jones, J Dobson, "Progress in applications of magnetic nanoparticles in biomedicine", *Journal of Physics D: Applied Physics*, 22, 42, 2009, 224001.
- [3]. S El-Badry, "Influence of Processing Parameters on the Magnetic Properties of Mn-Zn Ferrites", *Journal of Minerals and Materials Characterization and Engineering*, 10, 5, 2011, 397-407.
- [4]. E Auzans, D Zins, E Blums and R Massart, "Synthesis and properties of Mn-Zn ferrite ferrofluids", *Journal of Materials Science*, 34, 1999, 1253.
- [5]. FA Tourinho, R Franck, R Massart, "Aqueous ferrofluids based on manganese and cobalt ferrites", *Journal Materials Science*, 25, 1990, 3249.
- [6]. FA Lima, ME Saleta, RJS Pagliuca, MS Eleotério, J Fonseca Jr., BC Meyer, EM Bittar, NM Souza Neto, E Granado, "XDS: a flexible beamline for X-ray diffraction and spectroscopy at the Brazilian synchrotron", *Journal of Synchrotron Radiation*, 23, 6, 2016, 1538-1549.
- [7]. ME Saleta, MS Eleotério, A Mesquita, VR Mastelaro, E Granado, "Atomic pair distribution function at the Brazilian Synchrotron Light Laboratory: application to the $Pb_{1-x}La_xZr_{0.40}Ti_{0.60}O_3$ ferroelectric system", *Journal of Synchrotron Radiation*, 24, 5, 2017, 1098-1104.
- [8]. X Qiu, JW Thompson, SJL Billinge, "PDFgetX2: a GUI-Driven Program to Obtain the Pair Distribution Function from X-Ray Powder Diffraction Data", *Journal Applied Crystallography*, 37, 2004, 678.
- [9]. P Juhás, T Davis, CL Farrow and SJL Billinge, "PDFgetX3: a rapid and highly automatable program for processing powder diffraction data into total scattering pair distribution functions", *Journal Applied Crystallography*, 46, 2013, 560-566.
- [10]. CL Farrow, P Juhás, J W Liu, D Bryndin, E S Bozin, J Bloch, Th Proffen and S J L Billinge, PDFfit2 and PDFgui: computer programs for studying nanostructure in crystals, *Journal of Physics: Condensed Matter*, 19, 2007, 335219.
- [11]. C Larson, RB Von Dreele, "General Structure Analysis System", *Los Alamos National Laboratory*, <ftp://ftp.lanl.gov/public/gsas>, 2001.
- [12]. JABearden, AF Burr, "Reevaluation of X-Ray Atomic Energy Levels," *Rev Mod Phys*, 39, 1967, 125-142. <https://doi.org/10.1103/RevModPhys.39.125>
- [13]. GK Williamson, WH Hall, "X-Ray Line Broadening From Filed Aluminium And Wolfram", *Acta Metallurgica*, 1, 1953, 22-31.
- [14]. S Kuman, VD Mote, R Prakash, V, Kumar, "X-ray Analysis of α -Al₂O₃ Particles by Williamson-Hall Methods", *Materials Focus*, 5(6), 2016, 545.
- [15]. D Ko, K Poeppelmeier, D Kammler, G Gonzalez, T Mason, D Williamson, D Young, T Coutts, "Cation Distribution of the Transparent Conductor and Spinel Oxide Solution $Cd_{1+x}In_{2-x}Sn_xO_4$ " *J. Solid State Chem*, 163, 2002, 259-266.
- [16]. L Laffont, P Gibot, "High resolution electron energy loss spectroscopy of manganese oxides: Application to Mn₃O₄", *Materials Characterization*, 61, 2010, 1268-1273. [dx.doi.org/10.1016/j.matchar.2010.001](https://doi.org/10.1016/j.matchar.2010.001)
- [17]. K Mandal, S Mitra, P Anil Kumar, "Deviation from Bloch T^{3/2} law in ferrite nanoparticles", *Europhys Lett.*, 75 (4), 2006, 618-623. [10.1209/epl/i2006-10148-y](https://doi.org/10.1209/epl/i2006-10148-y)
- [18]. IJ Bruvera, P MensozaZélis, MP Calatayud, GF Goya, FH Sanches, "Determination of the blocking temperature of magnetic nanoparticles: The good, the bad and the ugly", *Journal of Applied Physics*, 118 (18), 2015, 184304. [doi:10.1063/1.4935484](https://doi.org/10.1063/1.4935484)
- [19]. JA Gomes, GM Azevedo, J Depeyrot, J Mestnik-Filho, FLO Paula, FA Tourinho, R Perzynski, "Structural, Chemical, and Magnetic Investigations of Core-Shell Zinc Ferrite Nanoparticles", *Journal of Physical Chemistry C*, 116, 2012, 24281-24291.
- [20]. FHM Da Silva, FG Silva, FLO Paula, JA Gomes, R Aquino, JMestnik-Filho, P Bonville, FPorcher, R Perzynski, J Depeyrot, "Local Structure Of Core-Shell MnFe₂O₄ based Nanocrystals: Cation Distribution and Valence States of Manganese Ions", *Journal of Physical Chemistry C*, 121, 2017, 8982-8991.
- [21]. F Agnoli, B Albouy, P Tailhades, A Rousset. "Manganites de fer de structure spinelle déformée à très fort champ coercitif. Exemple de l'oxyde lacunaire à valence mixte Mn_{1.7}Fe_{1.3}O_{4+δ}", *C. R. Acad. Sci. Paris*, t.2, série II 1999, 525-530.
- [22]. A Bianconi, MD Ariccia, PJ Durham, J B Pendry, "Multiple-Scattering Resonances and Structural Effects in the X-Ray-Absorption Near-Edge Spectra of Fe II and Fe III Hexacyanide Complexes", *Phys. Rev. B*, 26(12), 1992, 6502-6508.
- [23]. LS Kau, EI Solomon KO Hodgson, "XANES/EXAFS Study of the Copper Active Site in Methanol Synthesis", *J. Phys. C.*, 18(12), 1986, 289-292
- [24]. EC Sousa, HR Rechenberg, J Depeyrot, JA Gomes, R Aquino, FA Tourinho, V Dupuis, R Perzynski, "In-field Mossbauer study of disordered surface spins in core/shell ferrite nanoparticles", *Journal of Applied Physics*, 106, 2009, 093901. [http://dx.doi.org/10.1063/1.3245326](https://doi.org/10.1063/1.3245326)
- [25]. J Marx, H Huang, KSM Salih, WR Thiel, V Schunemann, "Spin canting in ferrite nanoparticles", *Hyperfine Interact* 237 (41), 2016. [10.1007/s10751-016-1241-5](https://doi.org/10.1007/s10751-016-1241-5)
- [26]. Xu Zuo, Aria Yang, Carmine Vittoria, and Vincent G. Harris, "Computational study of copper ferrite (CuFe₂O₄)", *Journal of Applied Physics*, 99, 2006, 08M909. [10.1063/1.2170048](https://doi.org/10.1063/1.2170048)